EUV spectra of Xe XVII–Xe XXI produced in charge-exchange collisions

R. D'Arcy,[1] O. Morris,[1] B. Li,[1] H. Ohashi,[2] S. Suda,[2] H. Tanuma,[2] S. Fujioka,[3] H. Nishimura,[3] K. Nishihara,[3] C. Suzuki,[4] T. Kato,[4] F. Koike,[5] and G. O'Sullivan[1]

[1]*University College Dublin, Belfield, Dublin 4, Ireland*

[2]*Department of Physics, Tokyo Metropolitan University, Hachioji, Tokyo 192-0397, Japan*

[3]*Institute of Laser Engineering, Osaka University, Suita, Osaka 565-0871, Japan*

[4]*National Institute for Fusion Science, Toki, Gifu 509-5292, Japan*

[5]*Physics Laboratory, School of Medicine, Kitasato University, Sagamihara, Kanagawa 228-8555, Japan*

(Received 4 November 2011; published 25 June 2012)

Charge-state-specific spectra produced from charge exchange collisions between xenon ions and helium target atoms using an ECR (electron cyclotron resonance) source have been recorded in extreme ultraviolet (EUV). At low target gas pressures, the spectra were produced after a single collision event involving electron capture by the projectile ion and in each case intense emission near 11 nm was observed. The spectra of Xe^{16+} to Xe^{20+} are compared with atomic structure calculations and the possible mechanisms for electron capture are discussed. There is some evidence that for lower charged ions the spectra in the 10–15 nm region result mainly from transfer excitation or ionization processes rather than direct single electron capture into high *nl* states.

DOI: 10.1103/PhysRevA.85.062513 PACS number(s): 32.30.−r

I. INTRODUCTION

In recent years there has been considerable interest in the extreme ultraviolet (EUV) spectra of xenon ions due to the importance of xenon plasmas as potential sources for high intensity operation at $\lambda = 13.5$ nm for EUV lithography (EUVL) and also as lower power metrology sources at this wavelength. Indeed, the first two microchip manufacturing tools designed for operation at this wavelength, the prototype or α-tools shipped in 2005 by Dutch semiconductor fabrication tool manufacturing giant ASML (Advanced Semiconductor Materials Lithography) initially used high power Xe-based plasma discharge sources developed by Philips [1]. In Xe, the emission at 13.5 nm is due to $5p \rightarrow 4d$ transitions in Xe XI and the detailed analysis of the spectrum has been published by Churilov *et al.* [2]. The energy levels and observed spectral lines of Xe in all stages of ionization, which were published before December 2002 have been compiled by Saloman [3]. The available data, however, is limited for higher charge states, in particular, for stages higher than Xe^{11+}. The EUV spectra of Xe recorded from laser produced plasmas, discharge plasmas, and electron-beam ion traps (EBITs) [4–6] are dominated by an intense unresolved transition array (UTA) [7] in the 11 nm region that results from overlapping $\Delta n = 0$, $n = 4 \rightarrow n = 4$ transitions from ions past Xe^{10+} which possess an open valence $4d$ subshell. Indeed, in a later study of the Xe XI spectrum, Fahy *et al.* [8] showed that the intensity available from $4d \rightarrow 4p$ and $4f \rightarrow 4d$ transitions greatly exceeded that from $5p \rightarrow 4d$ and this result was verified subsequently by Churilov *et al.* who succeeded in identifying over 200 lines of the $4d^7 5p + 4d^7 4f + 4p^5 4d^9 \rightarrow 4p^6 4d^8$ [9]. Analysis in the 10–11.5 nm region is complicated by the presence of many strong resonance lines from different ion stages. Although a large number of experimental studies of emission from Xe plasmas have been reported, these have rarely been performed using ion separation techniques. Moreover, opacity effects, which in an optically thick plasma can dramatically alter the ratio of intensity of high to low oscillator strength lines, as well as introducing a strong contribution from satellite emission [10] make intensity comparisons between theory and experiment extremely difficult. As a result, unambiguous line identification is almost impossible in regions of high line density. Thus, in order to understand the physics of EUV plasmas containing Xe, charge state specific spectra are an essential prerequisite.

It has been shown in the past that spectra of Xe resulting from collisions of moderately charged Xe ions with gases yield charge state specific spectra [11,12] and ion stage specific spectra of the emission contributing to the xenon UTA itself have recently been obtained using the charge-exchange method by Tanuma and co-workers [13,14]. In this work we report on the spectra of 16 to 20 times ionized xenon and concentrate on explaining the features obtained in the 10–15 nm region.

II. EXPERIMENT

The detailed description of the experimental setup has been given elsewhere and will only be briefly presented here [13]. Multiply charged ions were produced in a 14.25 GHz ECR (electron cyclotron resonance) ion source at Tokyo Metropolitan University. The Xe^{q+} ions were extracted with an electric potential of 20 kV and selected by a 110° double-focusing dipole magnet according to their mass-to-charge ratio. The ion beam was directed into a collision chamber, where it interacted with a target gas jet. The background pressure in the collision chamber was 6×10^{-6} Pa and the target gas pressure in the chamber was held at about 1×10^{-3} Pa during the measurements and was low enough to guarantee single-collision conditions. The primary ion beam, which was approximately 6 mm in diameter, had typically an electrical current of 0.1–2 μA as measured with a Faraday cup located behind the collision region. The EUV emission from the collision center was observed at 90° to the ion beam direction with a compact flat-field grazing-incidence spectrometer equipped with a toroidal collecting mirror and a 1200 lines/mm grating blazed at 100 nm. The detector was a liquid nitrogen cooled CCD (charge coupled device) camera

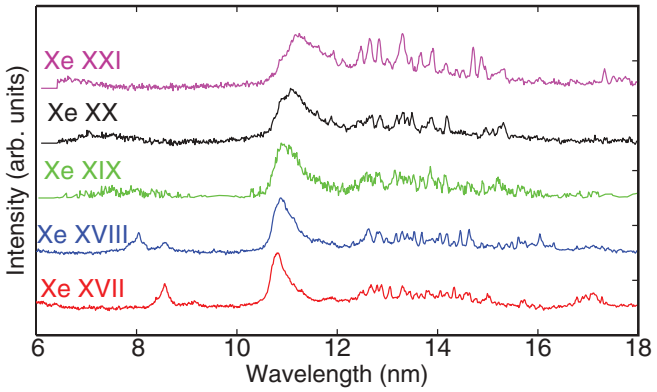

FIG. 1. (Color online) Spectra of Xe ions produced from charge exchange collisions with He target atoms using the Tokyo Metropolitan University ECR source. The spectrum of ion Xe^{q-1+} result from charge exchange collisions of Xe^{q+} ions with helium gas.

(C4880, Hamamatsu) which enabled an emission spectrum in the wavelength range of 6–24 nm to be accumulated simultaneously. A slit of width 200 μm placed between the mirror and the grating gave an instrumental resolution of approximately 0.03 nm. The uncertainty in the observed wavelength was estimated at 0.02 nm.

III. RESULTS

The spectra obtained at the ECR source are shown in Fig. 1. The spectra of ions $Xe^{(q-1)+}$ result from charge exchange collisions of Xe^{q+} ions with helium gas. Contributions from double collisions are assumed negligible given the low target pressure used in the experiment. Indeed, a previous study of collisions between highly charged Xe ions and He atoms with a target gas pressure one order of magnitude greater than the value used in the present work showed that there was an almost negligible contribution to the ionization stage of the projectile ion from double collisions [15]. In addition, this study further showed that the population of $Xe^{(q-2)+}$ ions resulting from single collision events involving double capture was negligible also.

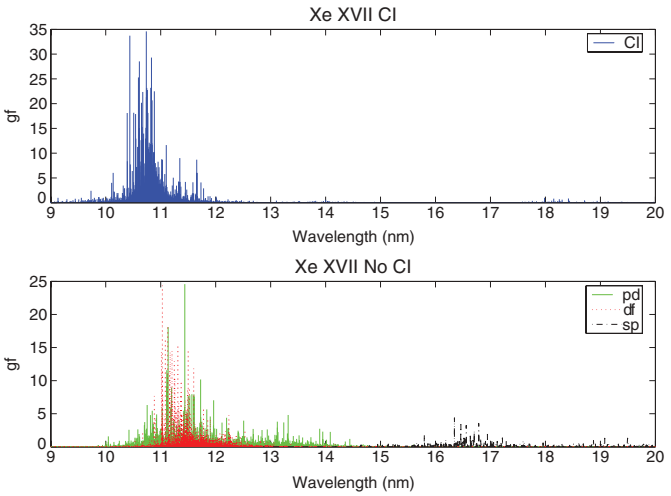

FIG. 2. (Color online) Comparison between CI (top) and non-CI (bottom) calculations for Xe XVII.

It is clearly seen from Fig. 1 that all of the spectra are dominated by an intense unresolved transition array in the 11 nm region. In the lower ion stages, Xe^{16+} and Xe^{17+}, which have open $4d$ subshells, the strongest features in the corresponding Xe XVII and Xe XVIII spectra are expected to result from resonance transitions, $4s^24p^54d^{n+1} + 4s^24p^64d^{n-1}4f \rightarrow 4s^24p^64d^n$ ($n = 2, 1$), with the possibility of transitions between excited states also making a contribution. In a recent study of the emission from Sn ions in stages from Sn^{14+} to Sn^{17+}, that is, with ground configurations $4p^6$ to $4p^3$, resonance transitions of the type $4p^{m-1}4d \rightarrow 4p^m$ were indeed present, but the dominant contribution came from transitions of the type $4s^24p^{m-1}4f + 4s^24p^{m-2}4d^2 + 4s4p^m4d \rightarrow 4s^24p^{m-1}4d$ [16]. In the present case, with increasing ion stage and the emergence of the open $4p$ subshell it is of interest to see if the same situation obtains for Xe as in

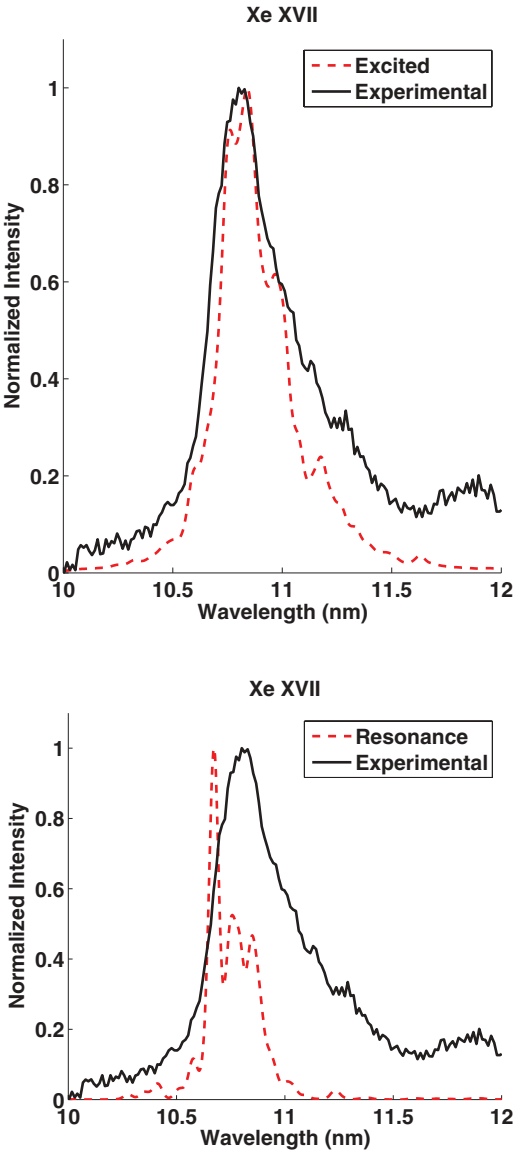

FIG. 3. (Color online) Comparison between a theoretical spectrum for excited to excited state transitions (a) and resonance transitions (b) of Xe XVII convolved with a Gaussian instrumental function and the obtained experimental spectrum of Xe XVII.

TABLE I. Observed and calculated wavelengths for the strongest observed lines of Xe XVII along with the calculated oscillator strengths (gf) (*res indicates a resonance line).

Transition	$\lambda_{\mathrm{Cowan(nm)}}$	$\lambda_{\mathrm{ECR(nm)}}$	gf
$(4p^5\,4d^3)^3F_4 \rightarrow (4p^6\,4d^2)^3F_4$	10.70_{res}		17.08
$(4p^6\,4d4f)^1H_5 \rightarrow (4p^6\,4d^2)^1G_4$	10.70_{res}	10.70	21.14
$4p^5\,4d^3)^1G_4 \rightarrow (4p^6\,4d^2)^1G_4$	10.71_{res}		18.68
$(4p^5\,4d^24f)^5H_7 \rightarrow (4p^5\,4d^3)^5F_6$	10.75	10.75	28.83
$(4p^5\,4d^24f)^3H_6 \rightarrow (4p^5\,4d^3)^3H_5$	10.77		21.18
$(4p^5\,4d^24f)^3G_5 \rightarrow (4p^5\,4d^3)^1H_5$	10.78	10.78	16.41
$(4p^6\,4d^24f)^3G_5 \rightarrow (4p^6\,4d^2)^3F_4$	10.78_{res}		20.74
$(4p^6\,4d^24f)^3G_3 \rightarrow (4p^6\,4d^2)^3F_3$	10.82_{res}	10.80	16.21
$(4p^5\,4d^24f)^1K_7 \rightarrow (4p^5\,4d^3)^1I_6$	10.83	10.83	28.70
$(4p^5\,4d^24f)^1H_5 \rightarrow (4p^5\,4d^3)^1G_4$	10.83		20.70
$(4p^5\,4d^24f)^1H_5 \rightarrow (4p^6\,4d4f)^1H_5$	10.94	10.95	17.00

Sn and explore if the contribution from excited to excited state transitions dominates these spectra also.

In slow collisions of highly charged ions with He gas a number of possible charge changing processes occur. Single electron capture (SEC), true double electron capture (TDC), and transfer ionization (TI) can take place. In both SEC and TI the projectile charge is reduced by one unit, while TDC results in a charge reduction of two. SEC can be regarded as the most dominant process [15,17,18] with the ratio of cross sections for transfer ionization to true single capture ranging from 0.24 to 0.56 [15]. In addition to these processes, Cederquist *et al.* have proposed a transfer excitation mechanism unique for two electron targets [19].

TABLE II. Observed and calculated wavelengths for the strongest observed lines of Xe XVIII along with the calculated oscillator strengths gf. (*res indicates a resonance line, Sugar indicates lines previously reported by Sugar *et al.* [25].)

Transition	$\lambda_{\mathrm{Cowan(nm)}}$	$\lambda_{\mathrm{ECR(nm)}}$	gf
$(4p^6\,4d^2)^2D_{3/2} \rightarrow (4p^6\,4d)^2D_{3/2}$	10.67_{res}	10.68	20.17
$(4p^6\,4d^2)^2F_{7/2} \rightarrow (4p^6\,4d)^2D_{5/2}$	10.73_{res}	10.72	14.42
		10.72_{Sugar}	
$(4p^6\,4d^2)^2D_{5/2} \rightarrow (4p^6\,4d)^2D_{5/2}$	10.82_{res}	10.81	11.70
		10.80_{Sugar}	
$(4p^6\,4f)^2F_{5/2} \rightarrow (4p^6\,4d)^2D_{3/2}$	10.95_{res}	10.95	10.56
		10.95_{Sugar}	

The energies of the capture states involved in the SEC process may be estimated from the classical over barrier model [20,21] and are dependent on the ionization potential of the projectile ion after capture (I^{q-1}) and target gas (I^T)

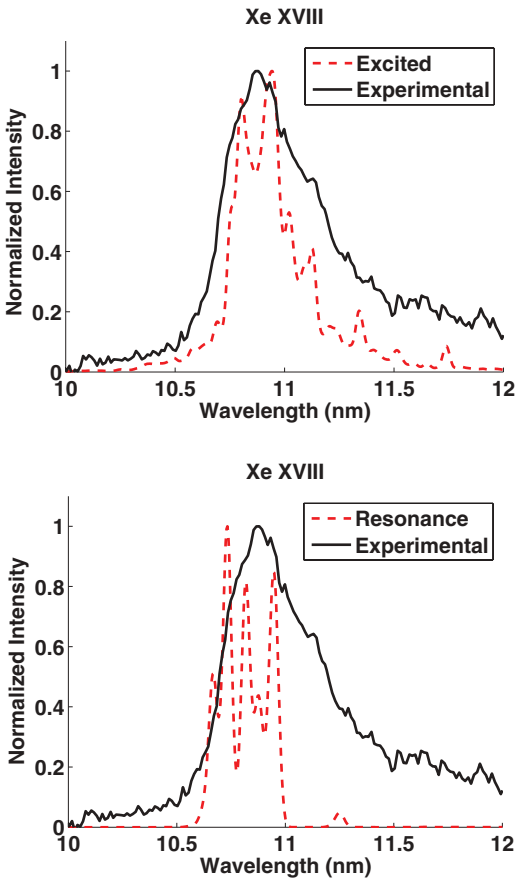

FIG. 4. (Color online) Comparison between a theoretical spectrum for excited to excited state transitions (a) and resonance transitions (b) of Xe XVIII convolved with a Gaussian instrumental function and the experimental spectrum of Xe XVIII.

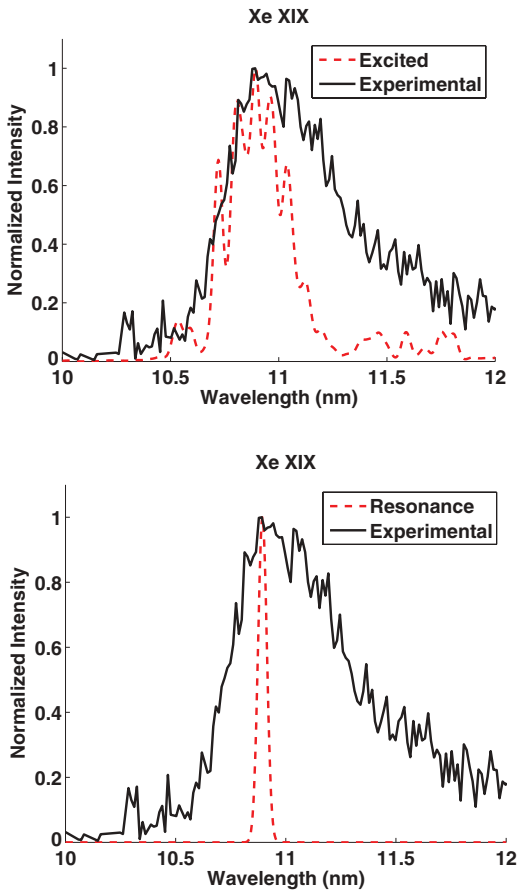

FIG. 5. (Color online) Comparison between a theoretical spectrum for excited to excited state transitions (a) and resonance transitions (b) of Xe XIX convolved with a Gaussian instrumental function and the experimental spectrum of Xe XIX.

according to

$$E_{\text{capture}} = I^{q-1} - (2\sqrt{q} + q)(2\sqrt{q} + 1)^{-1} I^{T}. \quad (1)$$

The model assumes that states exist in the vicinity of E_{capture}. The validity of Eq. (1) improves if there is a high density of states at this energy, that is, for capture into a high n state and for a compact high-q projectile, which is the case here.

As with the earlier work on Sn [16], calculations were performed for Xe^{16+}–Xe^{20+} using the Hartree-Fock with configuration interaction (HFCI) code of Cowan [22]. Configuration interaction (CI) effects in spectra where the strongest transitions satisfy $\Delta n = 0$ have been shown to be very significant because of the proximity of excitation energies [23,24]. In lower ion stages, when considering transitions from an open $4d$ subshell, excited state CI of the form $4p^6 4d^{m-1} 4f + 4p^5 4d^{m+1}$ is extremely important and produces a strong spectral narrowing. As with the our earlier work on Sn ions with $4p^m$ valence subshells the effects of CI in the upper basis states were explored here in some detail. In the present case calculations were performed for excited to excited $4p^{m-1}4f + 4p^{m-2}4d^2 \rightarrow 4p^{m-1}4d$ transitions ($4 \leqslant m \leqslant 6$). Again $4p^{m-1}4f + 4p^{m-2}4d^2$ CI was found to have a dramatic effect on the spectra of each ion stage in going from Xe XIX to Xe XXI. Just as in the case of resonance transitions from open $4d$ subshells, there is a radical redistribution of oscillator strength accompanied by a strong spectral narrowing and the calculations predict the appearance of a strong line group near 11 nm. However, in the previous study on CI effects in Sn ions [16] it was found necessary to allow for interaction with the lower energy core excited $4s4p^{m+1}$ configuration ($m < 6$) and this was also included in calculations for each of the ion stages here though the effects were found to be less pronounced in Xe presumably as the energy separation of the interacting configurations is greater in the present case.

For Xe XVII and Xe XVIII, calculations were performed for both resonance ($4s^2 4p^5 4d^{n+1} + 4s^2 4p^6 4d^{n-1} 4f^1 \rightarrow 4s^2 4p^6 4d^n$) and excited ($4s^2 4p^5 4d^n 4f^1 + 4s^2 4p^4 4d^{n+2} + 4s^1 4p^6 4d^{n+1} + 4s^2 4p^6 4d^{n-2} 4f^2 \rightarrow 4s^2 4p^5 4d^{n+1} + 4s^2 4p^6 4d^{n-1} 4f^1$) state transitions. Again CI effects in the upper state configuration were seen to have a very strong impact on the expected emission profile and lead to a dramatic spectral narrowing and enhancement of the highest gA values in both cases. In Fig. 2 where oscillator strengths (gf values) for each calculated line are plotted, we show the results of calculations with and without the inclusion of CI for Xe XVII.

The results of both the excited to excited state and resonance calculations were then convoluted with a Gaussian of width 0.03 nm to simulate the effects of instrumental broadening. In generating these theoretical spectra the Slater Condon

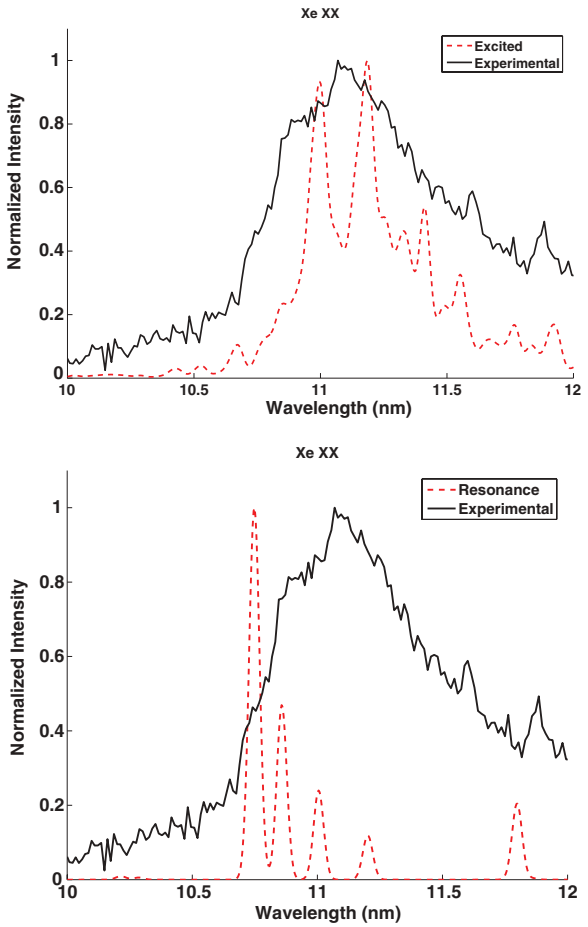

FIG. 6. (Color online) Comparison between a theoretical spectrum for excited to excited state transitions (a) and resonance transitions (b) of Xe XX convolved with a Gaussian instrumental function and the experimental spectrum of Xe XX.

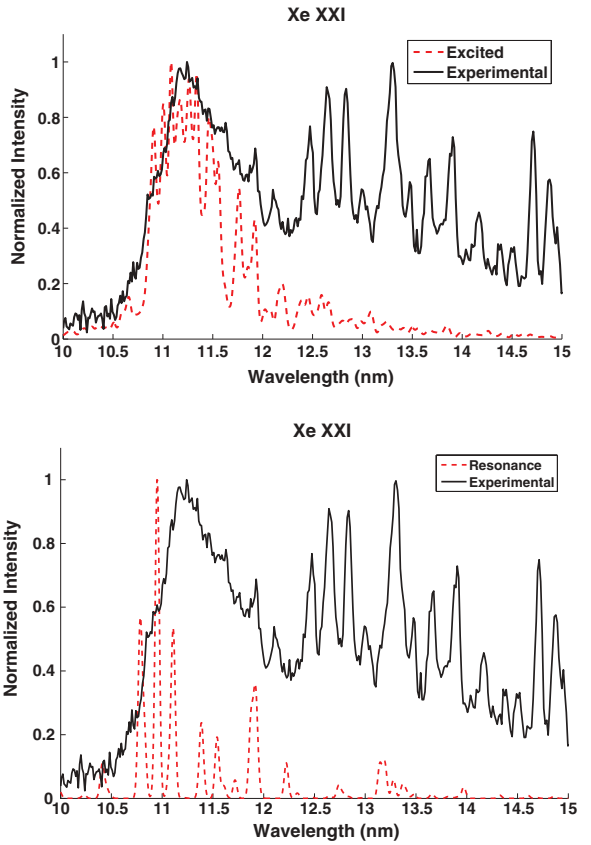

FIG. 7. (Color online) Comparison between a theoretical spectrum for excited to excited state transitions (a) and resonance transitions (b) of Xe XXI convolved with a Gaussian instrumental function and the experimental spectrum of Xe XXI.

parameters were reduced by 15% for excited to excited state transitions and 20% for resonance transitions, while the spin orbit parameters were left at their *ab initio* values. These scalings were found to give optimum agreement previously in the case of Sn.

A. Spectra of Xe XVII and Xe XVIII

The ground state of Xe XVII is Sr-like $4s^2 4p^6 4d^2$. From Fig. 3, where a comparison is made between the experimental and calculated spectra (No. of lines 2120), it was possible to find a shoulder at 10.7 nm and smaller peaks at 10.78 and 10.8 nm associated with the most intense calculated resonance transitions. However the dominant contribution comes from excited to excited state lines. In preparing these figures the excited and resonance spectra were shifted by $+0.07$ and $+0.03$ nm, respectively for optimum fitting. Table I lists the strongest predicted lines for both resonance transitions and those between the excited states. We have labeled the transitions according to the dominant composition of the upper level involved. The experimental values are tentative but correspond to definite line structure observed in the UTA.

For Xe XVIII, in comparing the experimental and calculated spectra (No. of lines 2333) the excited to excited state transitions are shifted by $+0.11$ nm for best fitting while the position of the resonance transitions remains unchanged. The results are presented for comparison in Fig. 4. Note that in both Figs. 3 and 4 the calculations reproduce the short wavelength structure of the UTA better than the longer wavelength end. This behavior may reflect the fact that the excited to excited transitions do not completely mirror the calculated intensity distribution due to selective population of upper levels but more likely stems from cascade processes whose contribution becomes more evident in higher stages, as will be discussed in the next section. Three lines have been classified by Sugar *et al*. [25] for this ion stage and these along with the strongest predicted lines from our calculations for resonance transitions to the ground configuration are listed in Table II, where the agreement is seen to be very good and gives further confidence in the choice of scaling factors.

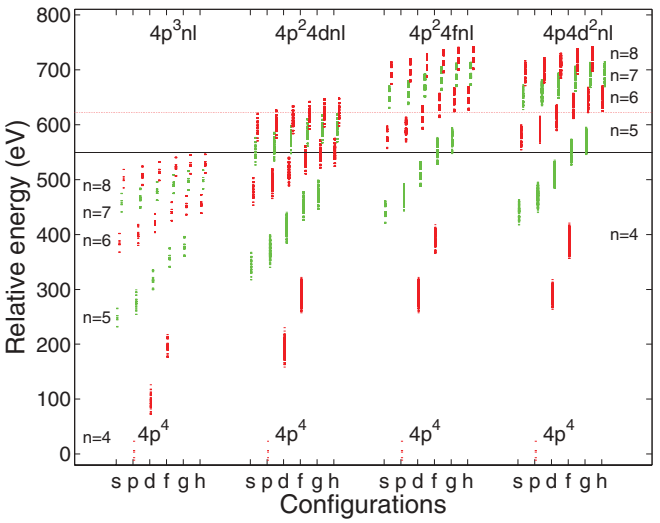

FIG. 8. (Color online) Energy-level diagram for Xe XXI: The energy predicted by the classical over barrier model is indicated by the black line and the ionization potential of Xe^{20+} is indicated by the dashed line.

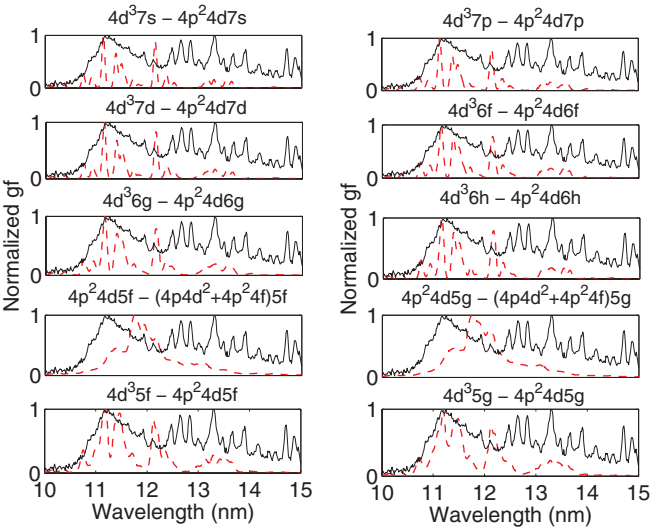

FIG. 9. (Color online) Comparison between theoretical spectra for excited to excited state transitions convolved with a Gaussian instrumental function and the experimental spectrum of Xe XXI.

B. Spectra of Xe XIX, Xe XX, and Xe XXI

With the emergence of the open $4p$ subshell in these ion stages it is seen that the spectra are still dominated by an unresolved transition array in the 11 nm region as evident from Fig. 1. As in the corresponding isoelectronic Sn ions, this behavior indicates that the spectra are dominated not by resonance $4p^{m-1}4d \rightarrow 4p^m$ lines but by transitions of the type $4s^2 4p^{m-1}4f + 4s^2 4p^{m-2}4d^2 + 4s4p^m 4d \rightarrow 4s^2 4p^{m-1}4d$, where again CI in the final state leads to strong spectral narrowing. However, a comparison between the calculated and experimental spectra for these transitions, Figs. 5–7, reveals

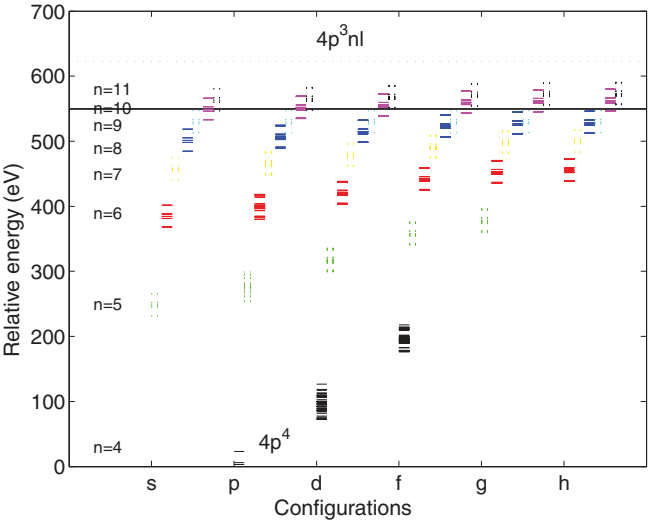

FIG. 10. (Color online) Energy-level diagram of $4p^3 nl$ configuration for Xe XXI.

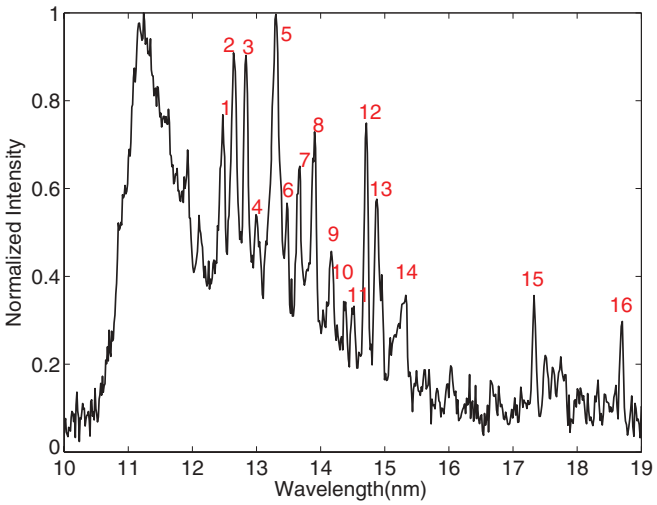

FIG. 11. (Color online) Experimental spectrum of Xe XXI with the identified lines from Table III.

that the agreement has decreased with increasing charge and the structure in the 12–15 nm region is as intense as the UTA itself. As the SEC cross section is known to increase linearly with q [18], it is possible to ascribe any such departures in our spectra to an increased contribution from cascade processes where selective population of excited levels leads to relatively intense emission from a number of lower oscillator strength transitions. Indeed such a scenario has to be invoked in order to explain the Xe XXI spectrum where the longer wavelength features are most pronounced. For this spectrum, while the $n = 4$ to $n = 4$ excited state contribution clearly exceeds that from resonance transitions to the ground state, the spectrum does not simply reflect the gf-value distributions and there is selective population of upper state terms resulting from these cascades which has the effect of broadening the overall array. The energies of the capture states were estimated using Eq. (1) and for Xe XXI the states populated with maximum probability by electron capture are those with energies close to 550 eV (Fig. 8). The ionization potential of Xe^{20+} whose ground state is $4p^4$ is indicated also on this figure and which predicts that configurations of the type $4p^3 10l$, $4p^2 4dnl$ ($nl = 7s, 7p, 7d, 6f, 6g$, and $6h$) and $(4p^2 4f + 4p4d^2)nl$ ($nl = 5f, 5g$) will be resonantly populated. For the preceding two ion stages the capture states are essentially the same.

A glance at Fig. 9 shows that transitions involving rearrangement of the $4p^2 4d$ or $(4p^2 4f + 4p4d^2)$ core essentially contribute to the UTA and that the latter will contribute mainly on the longer energy side. For decays involving the $4p^3 10l$ capture states, shown in exploded detail in Fig. 10, the resulting cascades can indeed contribute to the longer wavelength emission. For the lines labeled in Fig. 11, the possible originating configurations are tentatively identified in Table III.

IV. DISCUSSION AND CONCLUSION

The EUV spectra obtained in charge exchange collisions of Xe ions with helium exhibit an intense unresolved transition array in the 11 nm region. It was found that in interpreting these spectra that the dominant contribution came from excited to excited state transitions, exactly analogous to the previous observation for Sn [16] and thus seems to be generic for highly charged ions with $4p$ valence subshells. Such transitions were also found to dominate over resonance transitions here for Xe^{16+} and Xe^{17+}, which have $4d$ electrons in their outermost subshells. Moreover, it was necessary to allow for configuration interaction between different excited configurations built from $n = 4$ subshell electrons in all ion stages considered here. The dominance of these transitions in both Xe and Sn spectra would seem to imply that the upper doubly excited states are selectively populated in the charge exchange process either by a transfer excitation process in which electron capture is accompanied by the excitation of a $4p$ or $4d$ electron or a TI process in which the projectile ion autoionizes to a doubly excited state. It has been shown that in low energy electron scattering that the dielectronic

TABLE III. Possible originating configurations of Xe XXI (line 9 does not have a corresponding transition in the present calculations).

Label	Configurations for Xe XXI
1	$4p^3 12f \rightarrow 4p^3 7d$
2	$4p^3 11s \rightarrow 4p^3 7p$
3	$4p^3 11s \rightarrow 4p^3 7p, 4p^3 9d \rightarrow 4p^3 6f, 4p^3 12p \rightarrow 4p^3 7d$
4	$4p^3 9h \rightarrow 4p^3 6g, 4p^3 6g \rightarrow 4p^3 5f$
5	$4p^3 4d \rightarrow 4p^4, 4p^2 4d7s \rightarrow 4p^3 7s, 4p^2 4d7p \rightarrow 4p^3 7p, 4p^2 4d7d \rightarrow 4p^3 7d, 4p^2 4d6f \rightarrow 4p^3 6f,$ $4p^2 4d6g \rightarrow 4p^3 6g, 4p^2 4d6h \rightarrow 4p^3 6h, 4p^2 4d5f \rightarrow 4p^3 5f, 4p^2 4d5g \rightarrow 4p^3 5g$
6	$4p^3 9f \rightarrow 4p^3 6g, 4p^3 11f \rightarrow 4p^3 7d$
7	$4p^3 10d \rightarrow 4p^3 7p$
8	$4p^3 10d \rightarrow 4p^3 7p, 4p^3 12g \rightarrow 4p^3 7f$
9	
10	$4p^3 8p \rightarrow 4p^3 6d, 4p^3 8g \rightarrow 4p^3 6f, 4p^3 8g \rightarrow 4p^3 6h, 4p^3 11p \rightarrow 4p^3 7d, 4p^3 12d \rightarrow 4p^3 7f$
11	
12	$4p^3 10s \rightarrow 4p^3 7p$
13	$4p^3 10s \rightarrow 4p^3 7p, 4p^3 6p \rightarrow 4p^3 5d, 4p^3 12h \rightarrow 4p^3 7g$
14	$4p^3 10f \rightarrow 4p^3 7d, 4p^3 11g \rightarrow 4p^3 7f, 4p^3 7d \rightarrow 4p^3 6p, 4p^3 6p \rightarrow 4p^3 5d$
15	$4p^3 7f \rightarrow 4p^3 6d, 4p^3 12f \rightarrow 4p^3 7g$
16	$4p^3 6d \rightarrow 4p^3 5f, 4p^3 12s \rightarrow 4p^3 8p, 4p^3 9f \rightarrow 4p^3 7d$

recombination is greatly enhanced because of the large density of states resulting from open $n = 4$ subshells which leads to the dielectronic recombination rate exceeding that for radiative recombination by almost two orders of magnitude [26–28]. The agreement between calculated and experimental spectra decreases with increasing charge. The SEC cross section is known to increase linearly with q [18], and in the case of Xe XXI, it has been shown that the intense emission occurring on the long wavelength side of the UTA could arise from transitions within arrays produced by selective population of upper states resulting in cascades.

ACKNOWLEDGMENTS

This work was supported by MEXT, the Japanese Ministry for Education, Culture, Sports, Science and Technology and Science Foundation Ireland under Principal Investigator research Grant 07/IN.1/I1771.

[1] M. Carthout, R. Apetz, K. Bergmann, G. Derra, J. Jonkers, J. Pankert, and P. Zink, Proc. 5th Int. SEMATECH EUVL Symp., Barcelona, 18–24 Oct. 2006.
[2] S. S. Churilov, Y. N. Joshi, and J. Reader, Opt. Lett. **28**, 1478 (2003).
[3] E. B. Saloman, J. Phys. Chem. Ref. Data **33**, 765 (2004).
[4] G. O'Sullivan, J. Phys. B **15**, L765 (1982).
[5] M. A. Klosner and W. T. Silvast, J. Opt. Soc. Am. B **17**, 1279 (2000).
[6] K. Fahy, E. Sokell, G. O'Sullivan, A. Aguilar, J. M. Pomeroy, J. N. Tan, and J. D. Gillaspey, Phys. Rev. A **75**, 032520 (2007).
[7] J. Bauche and C. Bauche-Arnoult, Adv. At. Mol. Phys. **23**, 131 (1988).
[8] K. Fahy, P. Dunne, L. McKinney, G. O'Sullivan, E. Sokell, J. White, A. Aguilar, J. M. Pomeroy, J. N. Tan, B. Blagojević, E.-O. LeBigot, and J. D. Gillaspy, J. Phys. D: Appl. Phys. **37**, 3225 (2004).
[9] S. S. Churilov, Y. N. Joshi, J. Reader, and R. R. Kildiyarova, Phys. Scr. **70**, 126 (2004).
[10] A. Sasaki, K. Nishihara, M. Murakami, F. Koike, T. Kagawa, T. Nishikawa, K. Fujima, T. Kawamura, and H. Furukawa, Appl. Phys. Lett. **85**, 5857 (2004).
[11] M. O. Larsson, A. M. Gonzalez, R. Hallin, F. Heijkenskjöld, R. Hutton, A. Langereis, B. Nyström, G. O'Sullivan, and A. Wännström, Phys. Scr. **51**, 69 (1995).
[12] M. O. Larsson, A. M. Gonzalez, R. Hallin, F. Heijkenskjöld, B. Nyström, G. O'Sullivan, C. Weber, and A. Wännström, Phys. Scr. **53**, 317 (1996).
[13] H. Tanuma, H. Ohashi, E. Shibuya, N. Kobayashi, T. Okuno, S. Fujioka, H. Nishimura, and K. Nishihara, Nucl. Instrum. Methods Phys. Res. **235**, 331 (2005).
[14] H. Tanuma, H. Ohashi, S. Fujioka, H. Nishimura, A. Sasaki, and K. Nishihara, J. Phys Conf. Ser. **58**, 231 (2007).
[15] H. Andersson, G. Astner, and H. Cederquist, J. Phys. B **21**, L187 (1988).
[16] R. D'Arcy, H. Ohashi, S. Suda, H. Tanuma, S. Fujioka, H. Nishimura, K. Nishihara, C. Suzuki, T. Kato, F. Koike, J. White, and G. O'Sullivan, Phys. Rev. A **79**, 042509 (2009).
[17] J. Vancura, V. J. Marchetti, J. J. Perotti, and V. O. Krostroun, Phys. Rev. A **47**, 3758 (1993).
[18] N. Selberg, C. Biedermann, and H. Cederquist, Phys. Rev. A **54**, 4127 (1996).
[19] H. Cederquist, C. Biedermann, and N. Selberg, Phys. Rev. A **51**, 2191 (1995).
[20] A. Barany, G. Astner, H. Cederquist, H. Danared, S. Huldt, P. Hvelplund, A. Johnson, H. Knudsen, L. Liljeby, and K.-G. Rensfeld, Nucl. Instrum. Methods Phys. Res., Sect. B **9**, 397 (1985).
[21] A. Niehaus, J. Phys. B **19**, 2925 (1986).
[22] R. D. Cowan, *The Theory of Atomic Structure and Spectra* (University of California Press, Berkeley, 1981).
[23] F. Koike, S. Fritzsche, K. Nishihara, A. Sasaki, T. Kagawa, T. Nishikawa, K. Fujima, T. Kawamura, and H. Furukawa, J. Plasma Fusion Res. **7**, 253 (2006).
[24] P. Mandelbaum, M. Finkenthal, J. L. Schwob, and M. Klapisch, Phys. Rev. A **35**, 5051 (1987).
[25] J. Sugar, V. Kaufman, and W. L. Rowan, J. Opt. Soc. Am. B **9**, 1959 (1992).
[26] Y. B. Fu, C. Z. Dong, M. G. Su, and G. O'Sullivan, Chin. Phys. Lett. **25**, 927 (2008).
[27] M. Y. Song and T. Kato, J, Phys Conf. Ser. **72**, 012019 (2007).
[28] Y. B. Fu, C. Z. Dong, M. G. Su, F. Koike, G. O'Sullivan, and J. G. Wang, Phys. Rev. A **83**, 062708 (2011).